Inorg. Chem. **2007**, *46*, 7378–7386

Ternary Magnesium Rhodium Boride $Mg_2Rh_{1-x}B_{6+2x}$ with a Modified Y_2ReB_6-Type Crystal Structure

A. M. Alekseeva,[†,‡] A. M. Abakumov,[†,‡,§] P. S. Chizhov,[†,‡] A. Leithe-Jasper,[†] W. Schnelle,[†] Yu. Prots,[†] J. Hadermann,[§] E. V. Antipov,[‡] and Yu. Grin*[,†]

Max-Planck-Institut für Chemische Physik fester Stoffe, Nöthnitzer Strasse 40, 01187 Dresden, Germany, Chemistry Department, Moscow State University, Moscow 11992, Russia, and EMAT, University of Antwerp, Antwerp B-2020, Belgium

Received March 7, 2007

The new ternary magnesium rhodium boride $Mg_2Rh_{1-x}B_{6+2x}$ has been prepared by the reaction of the mixture of Mg powder, RhB, and crystalline boron in a Ta container sealed under argon. The crystal structure of $Mg_2Rh_{0.75(1)}B_{6.50(4)}$ is determined using single-crystal X-ray diffraction, electron diffraction, and high-resolution electron microscopy (space group *Pbam*, $a = 8.795(2)$ Å, $b = 11.060(2)$ Å, $c = 3.5279(5)$ Å, $Z = 4$, 630 reflections, $R_F = 0.045$). It represents a modified Y_2ReB_6 structure type with an unusual replacement of part of the Rh atoms by boron pairs located in the pentagonal channels parallel to the *c* axis. The pairs interconnect the neighboring planar boron nets into the 3D framework. The variation of the lattice parameters reveals a homogeneity range $Mg_2Rh_{1-x}B_{6+2x}$. The random distribution of the Rh atoms and boron pairs and the stabilizing effect of the boron pairs on the Y_2ReB_6 type structure motif are discussed using electronic band structure calculations and chemical bonding analysis with the electron localization function (ELF).

Introduction

The Y_2ReB_6 structure type is one of the prevalent structure types among the ternary transition metal borides with high boron content. The crystal structure of Y_2ReB_6 (space group *Pbam*, $a = 9.175$ Å, $b = 11.55$ Å, $c = 3.673$ Å)[1,2] can be described as an alternation along the *c*-axis of distorted close-packed layers of the metal atoms and planar boron nets formed by pentagonal, hexagonal, and heptagonal rings. This structure type is common for boron-rich ternary compounds of 4d and 5d transition metals (M) in the RE−M−B systems, where RE = U, Pu, Y, Gd, Tb, Dy, Ho, Er, Tm, Yb, and Lu and M = Mo, W, Tc, Re, Ru, and Os.[1−12] There are only a few representatives of the Y_2ReB_6 type among the ternary borides of rare-earth metals with 3d transition metals (Lu_2FeB_6,[13] Sc_2CrB_6,[14] $Lu_{1.34}V_{1.66}B_6$,[15] $Er(V_{0.77}Ta_{0.23})VB_6$[16]) and aluminum ($Sc_2AlB_6$,[17,18] Yb_2AlB_6,[19,20] Lu_2AlB_6[21]). In

* To whom correspondence should be addressed. E-mail: grin@cpfs.mpg.de.
† Max-Planck-Institut für Chemische Physik fester Stoffe.
‡ Moscow State University.
§ University of Antwerp.

(1) Kuz'ma, Yu. B.; Svarichevskaya, S. I. *Sov. Phys. Crystallogr.* **1972**, *17* (3), 569.
(2) Mikhalenko, S. I.; Kuz'ma, Yu. B.; Sobolev, A. S. *Sov. Powder Metall. Met. Ceram.* **1977**, *16*, 36.
(3) Rogl, P.; Nowotny, H. *Rare Earths Mod. Sci. Technol.* **1982**, *3*, 353.
(4) Rogl, P.; Delong, L. *J. Less-Common. Met.* **1983**, *91*, 97.
(5) Mikhalenko, S. I.; Kuz'ma, Yu. B. *Pol. J. Chem.* **2000**, *74*, 163.
(6) Chaban, N. F.; Kuz'ma, Yu. B. *Powder Metall. Met. Ceram.* **1999**, *38*, 458.
(7) Chaban, N. F.; Mikhalenko, S. I.; Kuz'ma, Yu. B. *Powder Metall. Met. Ceram.* **1998**, *37*, 635.
(8) Val'ovka, I. P.; Kuz'ma, Yu. B. *Sov. Powder Metall. Met. Ceram.* **1986**, *25*, 986.
(9) Chaban, N. F.; Mikhalenko, S. I.; Kuz'ma, Yu. B. *Powder Metall. Met. Ceram.* **2000**, *39*, 48.
(10) Chaban, N. F.; Mikhalenko, S. I.; Kuz'ma, Yu. B. *Powder Metall. Met. Ceram.* **2000**, *39*, 251.
(11) Rogl, P.; Potter, P. E.; Haines, H. R. *J. Nucl. Mater.* **1988**, *160*, 107.
(12) Leithe-Jasper, A.; Rogl, P.; Potter, P. E. *J. Nucl. Mater.* **1994**, *217*, 194.
(13) Dub, O. M.; Kuz'ma. Yu. B.; David, M. I. *Sov. Powder Metall. Met. Ceram.* **1991**, *344*, 681.
(14) Mykhalenko, S.; Babizhetskyj, V.; Kuz'ma, Yu. *J. Solid State Chem.* **2004**, *177*, 439.
(15) Chaban, N. F.; Mikhalenko, S. I.; Davidov, V. M.; Kuz'ma, Yu. B. *Powder Metall. Met. Ceram.* **2002**, *41*, 162.
(16) Kuz'ma, Yu. B.; Prots, Yu., Grin, Yu. *Z. Kristallogr.*—New Cryst. Struct. **2003**, *218*, 159.
(17) Okada, S.; Kudou, K.; Tanaka, T.; Shishido, T.; Gurin, V. N.; Lundström, T. *J. Solid State Chem.* **2004**, *177*, 547.
(18) Okada, S.; Tanaka, T.; Leithe-Jasper, A.; Michiue, Yu.; Gurin, V. N. *J. Solid State Chem.* **2000**, *154*, 49.
(19) Mikhalenko, S. I.; Kuz'ma, Yu. B.; Korsukova, M. M.; Gurin, V. N. *Izv. Akad. Nauk SSSR Neorg. Mater.* **1980**, *16*, 1941.
(20) Derkhachenko, L. I.; Gurin, V. N.; Korsukova, M. M.; Nechitailov, A. A.; Nechitailov, A. P.; Kuz'ma, Yu. B.; Chaban, N. F. *AIP Conf. Proc.* **1991**, *231*, 451.

10.1021/ic7004453 CCC: $37.00
Published on Web 08/09/2007

contrastto Re, Ru, and Os, compounds with Rh and Ir with this structure type are only known with scandium: Sc_2RhB_6 and Sc_2IrB_6.[22]

The interest in structures based on planar boron nets has significantly increased due to the important role of such nets for the superconducting behavior of MgB_2.[23] Several types of topologies of planar boron nets are known up to now, among them hexagonal graphite-like nets in the AlB_2 structure, the nets formed by pentagonal and heptagonal rings in $YCrB_4$[24] and $ThMoB_4$,[25] and the mixed boron nets corresponding to the Y_2ReB_6 structure type described above.

On the basis of the size criterion, the AMB_4 (A = alkaline-earth metal) borides with $YCrB_4$/$ThMoB_4$-type structure should be stable if $r_A/r_M > 1.30$, whereas the A_2MB_6 borides (Y_2ReB_6 structure type) require the r_A/r_M ratio to be lower than 1.30.[14] This points out the possibility of the formation of Y_2ReB_6-type borides in Mg−M−B systems with M = Rh, Ru, Re, and Os ($r_{Mg}/r_M > 1.16-1.19$).

In this work we report the synthesis and characterization of the new ternary boron compound of magnesium and rhodium with the Y_2ReB_6-like crystal structure.

Experimental Section

Starting Material and Synthesis Procedure. Magnesium powder (Alfa Aesar, 99.8%), rhodium powder (Chempur, 99.9%), and crystalline boron (Alfa Aesar, 99.999%) were used as the initial reagents. To improve the reactivity of the crystalline boron, the fraction with particle size smaller than 25 μm was selected for the preparation. All synthetic operations were performed in a glovebox under argon atmosphere (content of O_2 and $H_2O \leq 0.1$ ppm). The oxygen content in the initial materials was analyzed by the gas carrier hot extraction method (combined infrared and heat-conduction detector TC 436 DR/5, LECO). For the rhodium powder and the crystalline boron the oxygen content was found to be lower than the detection limit (0.038 wt %). An oxygen content of 0.05−0.20 wt % was found for different batches of the magnesium powder.

Taking into account the low reactivity and high melting points of Rh metal (T_m(Rh) = 1966 °C)[26] and crystalline boron ($T_m(B_{cr})$ = 2300 °C)[26], we used the rhodium monoboride (T_m = 1250 °C)[27] as a precursor for synthesis. Single-phase material with the composition RhB was prepared by arc-melting of the stoichiometric mixture of rhodium and boron powder under argon atmosphere. The obtained monoboride was ground in a tungsten carbide mortar and mixed with appropriate amounts of Mg powder and crystalline boron in an agate mortar, pressed into pellets, and sealed into tantalum containers (diameter 8 mm, length 25 mm). The tantalum containers were sealed into evacuated silica ampules and annealed at 850−1250 °C for 3−20 days with several intermediate regrindings in argon atmosphere. The ampules were finally quenched in water.

Table 1. Data Collection and Crystallographic Information for $Mg_2Rh_{0.75}B_{6.5}$

composition	$Mg_2Rh_{0.75}B_{6.5}$
space group	*Pbam*
a, Å	8.795(2)
b, Å	11.060(2)
c, Å	3.5279(5)
V, Å^3	343.2(2)
Z	4
radiation; wavelength, Å	Mo Kα; 0.71073
max. sinθ/λ	0.75
calculated density, g cm^{-3}	3.79
absorption coefficient, cm^{-1}	38.16
measured reflections	2537
independent reflections	630
R_{eq}	0.072
reflections used for refinement	531
no. of parameters refined	42
extinction coefficient	0.00021
R_F, wR_{F^2} for $F(hkl) \geq 6\sigma(F)$	0.045, 0.058

Differential Thermal Analysis (DTA). DTA was carried out in the range from room temperature to 1300 °C (STA 409, Netzsch, 30−60 mg/sample) in niobium containers sealed in argon atmosphere with a heating rate of 10 K/min.

X-ray Powder Diffraction. Phase identification and lattice parameter determination were performed from room-temperature X-ray powder diffraction data (Huber G670 Image Plate Guinier camera, Cu $K\alpha_1$ radiation, λ = 1.540598 Å) with LaB_6 as an internal standard (a = 4.15692 Å) for refinement of the unit cell parameters. The program packages WinCSD[28] and WinXPow[29] were used for processing of the powder data.

X-ray Single-Crystal Diffraction. Single crystals suitable for X-ray data collection were selected from a sample with nominal composition Mg_2RhB annealed at 1000 °C for 5 days with subsequent furnace cooling. The diffraction experiment was performed on a Rigaku AFC-7 four-circle system with Mercury CCD detector. Absorption correction was made using a multiscan procedure. Crystallographic information and details on the data collection are given in Table 1. The program package WinCSD[28] was used for the structure solution and refinement.

Metallography and Energy Dispersive X-ray Analysis (EDX). The metallographic investigation was performed on polished samples with a Zeiss Axiotec 100 optical microscope equipped with polarizer and analyzer and located in an argon-filled glovebox.[30]

The chemical compositions of the bulk sample and of the single crystal used for the diffraction experiment were analyzed with a Philips XL30 scanning electron microscope equipped with an EDAX Phoenix detector. EDXS measurements were performed with a standardless method on Mg *K* and Rh *L* lines at 5−7 points for each phase.

Measurements of Physical Properties. The magnetic susceptibility was measured in a SQUID magnetometer (Quantum Design MPMS-XL7) in various external fields down to 1.8 K on a small polycrystalline sample. A correction for a ferromagnetic trace impurity (corresponding to <10 μg of Fe metal/g) was done using the Honda-Owen extrapolation. The electrical resistivity was determined in a standard dc four-point setup on a bar-shaped sintered powder sample in a temperature range between 3.8 and 320 K.

(21) Okada, S.; Yu, Y.; Lundström, T.; Kudou, K.; Tanaka, T. *Jpn. J. Appl. Phys.* **1996**, *35*, 4718.
(22) Salamakha, P. S.; Rizzoli, C.; Salamakha, L. P.; Sologub, O. L.; Gonçalves, A.; Almeida. M. *J. Alloys Compd.* **2005**, *396*, 240.
(23) Nagamatsu, J.; Nakagava, N.; Muranaka, T.; Zenitani, Y.; Akimitsu, J. *Nature* **2001**, *410*, 63.
(24) Kuz'ma, Yu. B. *Kristallografiya* **1970**, *15*, 372 (in Russian).
(25) Rogl, P.; Nowotny, H. *Monatsh. Chem.* **1974**, *105*, 1082.
(26) Emsley, J. *The elements*; Oxford Chemistry Guides: London, 1991.
(27) Oborowski, W. *Metall (Isernhagen, Ger.)* **1963**, *17*, 108.
(28) Akselrud, L. G.; Zavalii, P. Yu.; Grin, Yu.; Pecharsky, V. K.; Baumgartner, B.; Wölfel, E. *Mater. Sci. Forum* **1993**, *133−135*, 335.
(29) *STOE WinXPow*, version 2.08; STOE & Cie GmbH: Darmstadt, Germany, 2003.
(30) Burkhardt, U. *Scientific report 2001/2002*; Max-Planck.Institut für Chemische Physik fester Stoffe: Dresden, Germany, Jan 2003; p 39.

Calculation Procedure. The electronic structure of the $Mg_2Rh_{1-x}B_{6+2x}$ compound was calculated for two ordered models: Mg_2RhB_6 and $Mg_2Rh_{0.5}B_7$. For the first case the symmetry coincides with the symmetry of the original structure (*Pbam*); for the second case an ordered model with lower symmetry ($P2_1am$) was employed. The TB-LMTO-ASA[31] program package was used for the calculations; a Barth−Hedin[32] exchange-correlation potential was applied. The calculations were made for 16 *k*-points in the irreducible wedge of the Brillouin zone. The integration over the Brillouin zone was performed using the tetrahedron method with 72 inequivalent tetrahedra.

Both mentioned models are nearly close-packed, so it was possible to avoid empty spheres addition in all cases.[33] The radii of the Rh spheres were 1.563 and 1.556 Å; the Mg sphere radii varied in the range 1.600−1.910 Å for different positions in different structures, and the B sphere radii were varied in the range 0.958−1.038 Å. A basis set containing Mg(3*s*,3*p*), Rh(5*s*,5*p*,4*d*), and B(2*s*,2*p*) orbitals was employed for the self-consistent calculations with Mg(3*d*), Rh(4*f*), and B(3*d*) functions being downfolded.

The electron localization function (ELF, η) was evaluated according to Ref. 34 with the intrinsic procedure of the TB-LMTO-ASA package. To get more insight into the bonding situation in $Mg_2Rh_{1-x}B_{6+2x}$, the topology of the ELF was analyzed using the program BASIN,[35] with subsequent integration of the electron density (ED) inside the corresponding ELF basins, like it was proposed for the electron density within the AIM approach.[36] This procedure allows determining the electron counts for the atomic core shells and the bonding attractors.

Transmission Electron Microscopy. Electron diffraction patterns were recorded on a Phillips CM20 microscope, and high-resolution images, on a JEOL 4000 EX. Simulations were made using the software package MacTempas.

Results and Discussion

The best nearly single-phase sample of the new phase, most suitable for the physical measurements, was obtained by heat treatment of a mixture of RhB, Mg, and B with the initial composition $Mg_2Rh_{0.5}B_7$ at 1000 °C for 8 days and then at 1200 °C for 8 days followed by quenching in water. The X-ray powder diffraction data (Figure 1) show the presence of the new orthorhombic phase with a small amount of MgO (~3%, originating from the initial Mg powder) and a few additional nonindexed peaks with maximum intensity of ~3% of the strongest observed reflection. The X-ray powder diffraction pattern was indexed on a primitive orthorhombic lattice with unit cell parameters $a = 8.752(1)$ Å, $b = 11.056(2)$ Å, and $c = 3.5874(7)$ Å. The lattice parameters, observed extinction conditions, and intensity distribution indicated that the new phase belongs to the Y_2ReB_6 structure type. From metallographic analysis and EDXS investigation, the majority phase with the Mg/Rh ratio of 3.4(3) was found together with a small amount of MgO and an additional phase of which the composition could not be precisely determined due to the very small particle size. Thus, the EDXS analysis shows a higher magnesium/rhodium ratio in the new phase compared to the A/M = 2 ratio in the Y_2ReB_6-type structure. No other elements were detected in the products.

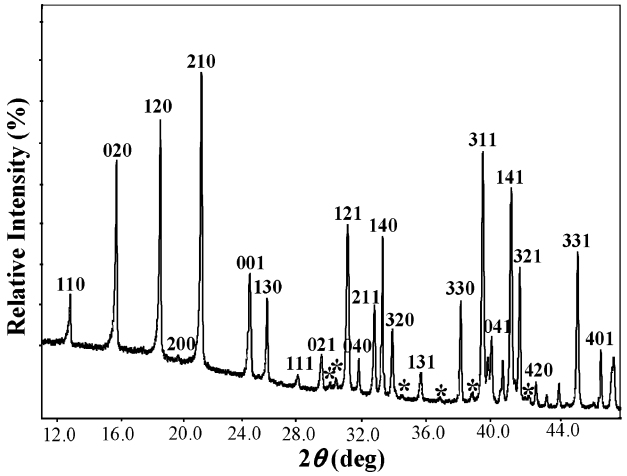

Figure 1. X-ray powder diffraction pattern of $Mg_2Rh_{0.5}B_7$ (thermal treatment: 8 days at 1000 °C + 8 days at 1200 °C). Reflections of the admixture phases are marked with stars.

The crystal structure of $Mg_2Rh_{0.75}B_{6.5}$ was determined using X-ray single-crystal diffraction data (cf. Experimental Section). The atomic coordinates from the crystal structure of Y_2ReB_6 were chosen as starting values for the refinement. However, the refinement resulted in relatively large values of the reliability factors ($R_F = 0.090$, $wR_{F^2} = 0.144$) and in an unusually high value of the atomic displacement parameter (ADP) for the Rh position. This suggested the presence of vacancies in the Rh position. The EDXS analysis of the single crystal revealed the Mg/Rh ratio of 2.74(5), in agreement with the Rh deficiency. Refinement of the occupancy factor for the Rh position led to the value of 0.75(1). With this occupancy the ADP for the Rh position decreased to a reliable value. The reliability factors also decreased to $R_F = 0.059$ and $wR_{F^2} = 0.076$. However, additional maxima of the difference Fourier map (3.2 $e^-/Å^3$) were found above and below the Rh atom along [001] (Figure 2a). The refinement of the ADP for the Rh atom in anisotropic approximation did not reduce these residual peaks in the difference Fourier map. The distances between the positions of the additional maxima and between these positions and neighboring boron atoms belonging to the existing planar nets at $z = 0.5$ were between 1.72 and 1.77 Å. Such interatomic distances are typical for boron−boron contacts. Therefore, it was assumed that the residual peaks of electron density correspond to a pair of boron atoms (B7). The center of mass for the B−B pair occupies the same position as the Rh atom. Finally, the occupancy and displacement parameters for the Rh atom were refined simultaneously with occupancy for the boron position B7. B_{iso}(B7) was fixed at 0.5 $Å^2$ because of the instability of the refinement caused by large difference in scattering power between 1.25 for 0.25 B and 33.75 electrons for 0.75 Rh

(31) Jepsen, O.; Burkhardt, A.; Andersen, O. K. *The TB-LMTO-ASA Program*, version 4.7; Max-Planck-Institut für Festkörperforschung: Stuttgart, Germany, 1999.
(32) Barth, U.; Hedin, L. *J. Phys. C* **1972**, *5*, 1629.
(33) Andersen, O. K.; *Phys. Rev. B* **1975**, *12*, 3060.
(34) Savin, A.; Flad, H. J.; Preuss, H.; von Schnering, H. G. *Angew. Chem.* **1992**, *104*, 185; *Angew. Chem., Int. Ed.* **1992**, *31*, 185.
(35) Kohout, M. *Basin*, version 2.3; Max-Planck-Institut für Chemische Physik fester Stoffe: Dresden, Germany, 2001.
(36) Bader, R. F. W. *Atoms in molecules: a quantum theory*; Oxford Univ. Press: Oxford, U.K., 1999.

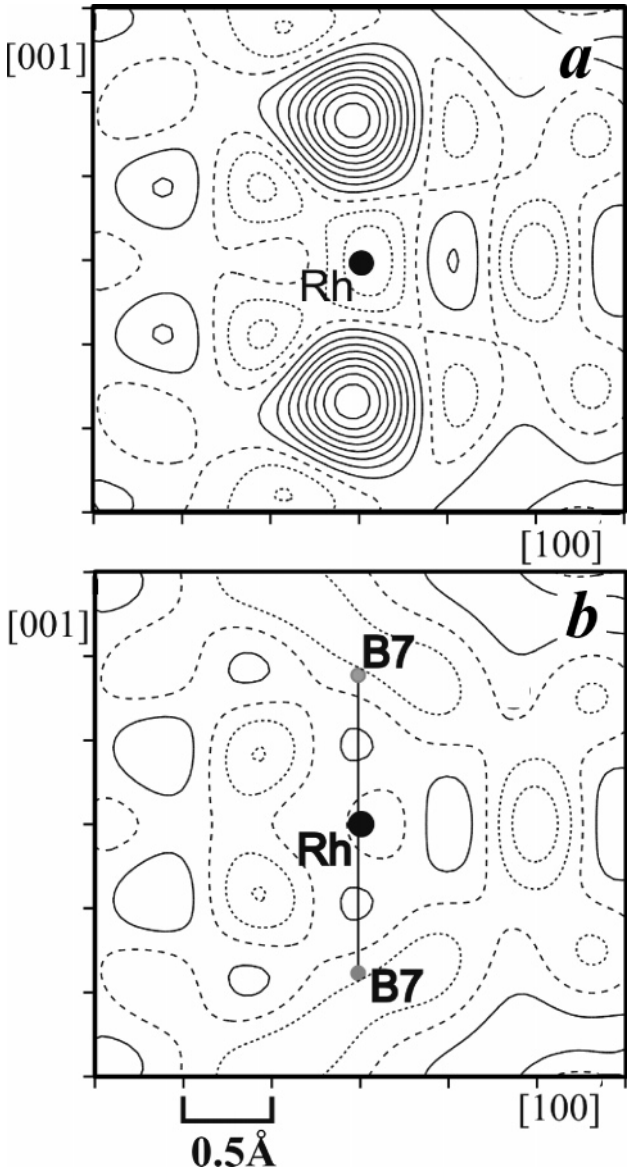

Figure 2. Difference electron density map in the vicinity of the Rh atom position (isolines are drawn with a step of 0.3 $e^-/Å^3$, zero line is dashed): (a) without boron atoms in the B7 position; (b) with B7 atoms.

located close to each other. Such refinement converged at occupancy factors for the Rh and B7 positions of 0.75(1) and 0.25(2), respectively, and at significantly lower values for the reliability factors ($R_F = 0.045$, $wR_{F^2} = 0.058$). The value of the largest residual peak of electron density decreased to 0.98 $e^-/Å^3$ (Figure 2b). The final atomic parameters are listed in Table 2, and the interatomic distances are given in Table 3.

As a result of the structure refinement, the composition of the compound has to be described as $Mg_2Rh_{1-x}B_{6+2x}$, where x corresponds to the occupancy factor of the B7 position. The Mg/Rh ratio obtained from the structure refinement is 2.67(3), within one esd equal to the EDXS data (Mg/Rh = 2.74(5)) on the investigated single crystal. The final composition is then described as $Mg_2Rh_{0.75(1)}B_{6.50(4)}$. The bulk powder material is, according to EDXS, even more Rh-depleted: $Mg_2Rh_{0.60(5)}B_{6.80(5)}$.

Simultaneous occupation of both the (x, y, 0.249) and (x, y, 0.751) B7 sites (parts of the 8*i* position related by a mirror plane) by boron atoms with a probability of 25% and Rh site with a probability of 75% is equivalent to a presence of either the B−B pair or the rhodium atom. If either only the (x, y, 1/4) or only the (x, y, 3/4) position is occupied, the obtained occupancies results in a simultaneous presence of the Rh atoms and the B atoms either above or below the Rh with nonphysically short RhB distances. The ordered distribution of the Rh atoms and boron pairs may result in a possible superstructure. The reciprocal lattice was investigated using electron diffraction on the sample $Mg_2Rh_{0.6}B_{6.8}$. The electron diffraction patterns taken along the most relevant zone axes are shown in Figure 3. All patterns can be completely indexed with a primitive orthorhombic lattice and the unit cell parameters determined from X-ray powder diffraction. The following reflection conditions were observed: $0kl$, $k = 2n$; $h0l$, $h = 2n$. These conditions are compatible with space group *Pbam*. The forbidden reflections $0k0$ with $k \neq 2n$ and $h00$ with $h \neq 2n$ present on the [001] pattern; both are caused by multiple diffraction, as was confirmed by the absence of these reflections on the [100] and [010] patterns. No signs of superstructure formation through ordered distribution of rhodium atoms and boron pairs were observed, confirming the results of the single-crystal structure determination.

The crystal structure of $Mg_2Rh_{1-x}B_{6+2x}$ (Figure 4a) reproduces in general the features of the Y_2ReB_6 structure type. It can be described as a stacking the boron nets along [001] which are sandwiched by the metal atoms solely located above and below the boron ring centers. One-quarter of the Rh atoms are replaced by the B−B pairs. The plane boron nets are formed of pentagonal, hexagonal, and heptagonal rings (Figure 4b). The neighboring plane nets can be interconnected by the $(B7)_2$ pair instead of Rh, which leads to the formation of pentagonal-pyramidal units (Figure 4c). These units are parts of the icosahedral B_{12} clusters in the crystal structure of elemental α-boron (Figure 4d) or other boron-rich phases like MgB_4 (Figure 4e).[37−39]

The partial hierarchical replacement is relatively rare among the crystal structures of intermetallic compounds. The atom-by-pair replacement was found, e.g., in the $TbCu_7$ compound.[40] The atom-by-triangle substitution was observed recently in several gallides: $Eu_{1-x}Ga_{2+3x}$;[41] $Eu_{3-x}Ga_{8+3x}$;[42] $Sr_{3-x}Ga_{8+3x}$;[43] $YbGa_{2.63}$.[44]

The boron−boron distances within the planar nets vary in the range from 1.68 to 1.83 Å. This is comparable with

(37) Matkovich, V. I. *Boron and Refractory Borides*; Springer-Verlag: Berlin, Heidelberg, Germany, 1977.
(38) Hoard, J. L.; Hughes, R. E. *The Chemistry of Boron and Its Compounds*; Muetterties, E. L., Ed.; J. Wiley: New York, London, Sydney, 1967; p 25.
(39) Guette, A.; Naslain, R.; Galy, J. *C. R. Acad. Sc. Paris* **1972**, *275*, 41.
(40) Buschow, K. H. J.; Groot, A. S. *Acta Crystallogr.* **1971**, *B27*, 1085.
(41) Sichevich, O.; Ramlau, R.; Giedigkeit, R.; Schmidt, M.; Niewa, R.; Grin, Yu. *Abstracts of the 13th International Conference on Solid State Compounds of Transition Elements*, Stresa, Italy, 2000; p O-13.
(42) Sichevich, O.; Prots, Yu.; Grin, Yu. *Z. Kristallogr.*—New Cryst. Struct. **2006**, *221*, 265.
(43) Haarmann, F.; Prots, Yu.; Göbel, S.; von Schnering, H. *Z. Kristallogr.*—New Cryst. Struct. **2006**, *221*, 257.
(44) Cirafici, S.; Fornasini, M. L. *J. Less-Common Met.* **1990**, *163*, 331.

Table 2. Atomic Coordinates and Displacement Parameters (in Å^2) for $Mg_2Rh_{0.75}B_{6.5}$

atom	occ	site	*x*/*a*	*y*/*b*	*z*/*c*	$B_{eq/iso}$[a]
Mg1		4*g*	0.6794(4)	0.0846(3)	0	1.32(8)
Mg2		4*g*	0.0547(4)	0.1265(3)	0	0.76(7)
Rh	0.75(1)	4*g*	0.3594(1)	0.1809(1)	0	0.63(2)
B1		4*h*	0.870(1)	0.1825(9)	1/2	0.6(1)
B2		4*h*	0.248(1)	0.0783(9)	1/2	0.8(1)
B3		4*h*	0.906(1)	0.0256(8)	1/2	0.5(1)
B4		4*h*	0.446(1)	0.0640(8)	1/2	0.3(1)
B5		4*h*	0.203(1)	0.2395(9)	1/2	0.4(1)
B6		4*h*	0.522(1)	0.2121(8)	1/2	0.4(1)
B7	0.25(2)	8*i*	0.359(2)	0.179(2)	0.249(7)	0.5[b]

atom	B_{11}[c]	B_{22}	B_{33}	B_{12}	B_{12}	B_{13}
Mg1	0.47(3)	0.48(3)	0.94(3)	0.01(3)	0	0
Mg2	1.8(2)	0.9(1)	1.2(1)	0.1(1)	0	0
Rh	0.6(1)	0.7(1)	1.1(1)	0.14(9)	0	0

[a] $B_{eq} = 1/3[a^{*2}a^2B_{11} + b^{*2}b^2B_{22} + c^{*2}c^2B_{33} + 2aba^*b^*(\cos\gamma)B_{12} + 2aca^*c^*(\cos\beta)B_{13} + 2bcb^*c^*(\cos\alpha)B_{23}]$; the displacement parameters for boron atoms were refined isotropically. [b] The isotropic displacement parameter for B7 atom was fixed (cf. text). [c] Anisotropic displacement parameter is defined as $\exp[-1/4(a^{*2}h^2B_{11} + b^{*2}k^2B_{22} + c^{*2}l^2B_{33} + 2a^*b^*hkB_{12} + 2a^*c^*hlB_{13} + 2b^*c^*klB_{23})]$.

Table 3. Selected Interatomic Distances (Å) for $Mg_2Rh_{0.75}B_{6.5}$

atoms	distance	atoms	distance
Mg1−B2	2.601(8)	Rh−B6	2.297(6)
Mg1−B5	2.634(8)	Rh−B2	2.315(6)
Mg1−B6	2.649(7)	Rh−B4	2.316(6)
Mg1−B4	2.651(7)	Rh−B1	2.324(7)
Mg1−B1	2.663(7)	Rh−B5	2.329(6)
Mg1−B4	2.716(7)		
Mg1−B3	2.740(7)	B1−B5	1.70(1)
Mg1−Rh	2.956(4)	B1−B3	1.76(1)
Mg1−Rh	3.009(4)	B1−B7	1.77(2)
Mg1−Rh	3.039(4)	B1−B6	1.77(1)
Mg1−Mg2	3.305(5)		
Mg1−Mg2	3.333(5)	B2−B7	1.72(2)
Mg1−Mg2	3.378(5)	B2−B4	1.75(1)
Mg1−Mg1	3.5279(5)	B2−B3	1.78(1)
Mg1−Mg1	3.669(5)	B2−B5	1.83(1)
Mg2−B3	2.462(7)	B3−B3	1.75(1)
Mg2−B3	2.463(7)		
Mg2−B1	2.477(7)	B4−B4	1.71(1)
Mg2−B2	2.507(7)	B4−B7	1.73(2)
Mg2−B5	2.525(7)	B4−B6	1.77(1)
Mg2−B6	2.526(7)		
Mg2−Rh	2.736(4)	B5−B6	1.68(1)
Mg2−Rh	2.747(4)	B5−B7	1.76(2)
Mg2−B7	2.88(2)		
Mg2−B7	2.89(2)	B6−B7	1.72(2)
Mg2−Mg2	2.959(5)	B7−B7	1.76(4)
Mg2−Mg2	3.5279(5)		

the double covalent radius of boron (r_{cov}(B) = 0.88 Å)[26]. The distances within the boron pair (B7−B7) and between the B7 atoms and boron atoms from the boron nets are also comparable with $2r_{cov}$(B). The distances between the Mg and Rh atoms are in accord with the sum of the metallic radii (r(Mg) = 1.600 Å, r(Rh) = 1.345 Å)[26]. The Mg−B and Rh−B distances are approximately equal or slightly larger than the sum of the radii.

Random distribution of the B−B pairs and the Rh atoms in their positions within the (001) plane was proven by HREM observation along [001]. On the [001] HREM image of $Mg_2Rh_{0.6}B_{6.8}$ (Figure 5a) the dark spots correspond to the projection of the pentagonal rings of the boron nets; cf. the theoretical image calculated at defocus $\Delta f = -50$ Å and thickness $t = 40$ Å (inset in Figure 5a) using the atomic coordinates from Table 2. The dark spots corresponding to the pentagonal channels are occasionally absent (as indicated by the arrows in Figure 5b). This corresponds to the positions preferentially occupied by the B−B pairs rather than the Rh atoms. The missing spots are randomly distributed, confirming the lack of ordering in the (001) plane. The remarkable difference in contrast occurs due to the drastic difference in scattering power between B and Rh (Figure 5c).

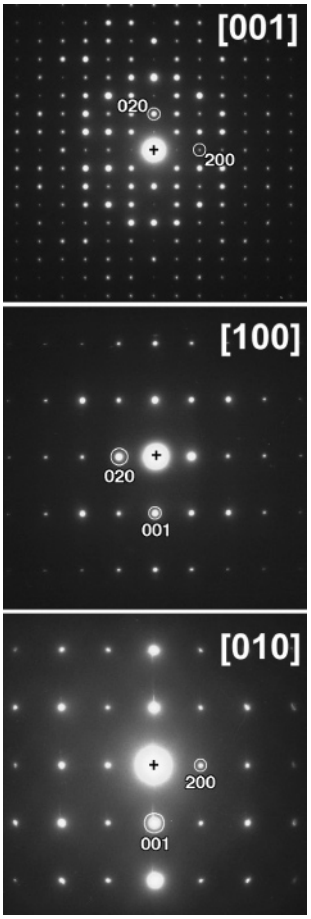

Figure 3. Electron diffraction patterns of $Mg_2Rh_{0.6}B_{6.8}$.

One may expect that the substitution of rhodium by boron pairs results in the formation of a $Mg_2Rh_{1-x}B_{6+2x}$ solid solution. The homogeneity range of this solid solution was investigated. The samples prepared from the mixture of RhB, Mg, and crystalline boron with initial compositions $Mg_2Rh_{1-x}B_{6+2x}$ ($0 \le x \le 0.9$) were consistently annealed at 1000, 1200, and 1100 °C for 7−10 days with intermediate regrindings. Despite the long annealing time, most of the prepared samples contained minor admixtures of one or two ternary phases (e.g., $Mg_{1-x}RhB$,[45] $Mg_3Rh_5B_2$[46]) and binary phases MgO, $Mg_{44}Rh_7$,[47] MgB_4,[39] and MgB_2.[23] Nevertheless, the lattice parameters of the $Mg_2Rh_{1-x}B_{6+2x}$ phase vary with

(45) Alekseeva, A. M.; Abakumov, A. M.; Leithe-Jasper, A.; Schnelle, W.; Prots, Yu.; Hadermann, J.; Van Tendeloo, G.; Antipov, E. V.; Grin, Yu. *Z. Anorg. Allg. Chem.* **2005**, *631*, 1047.
(46) Nagelschmitz, E. A.; Jung, W.; Feiten, R.; Müller, P.; Lueken, H. *Z. Anorg. Allg. Chem.* **2001**, *627*, 523.
(47) Westin, L. *Chem. Scr.* **1971**, *1*, 127.

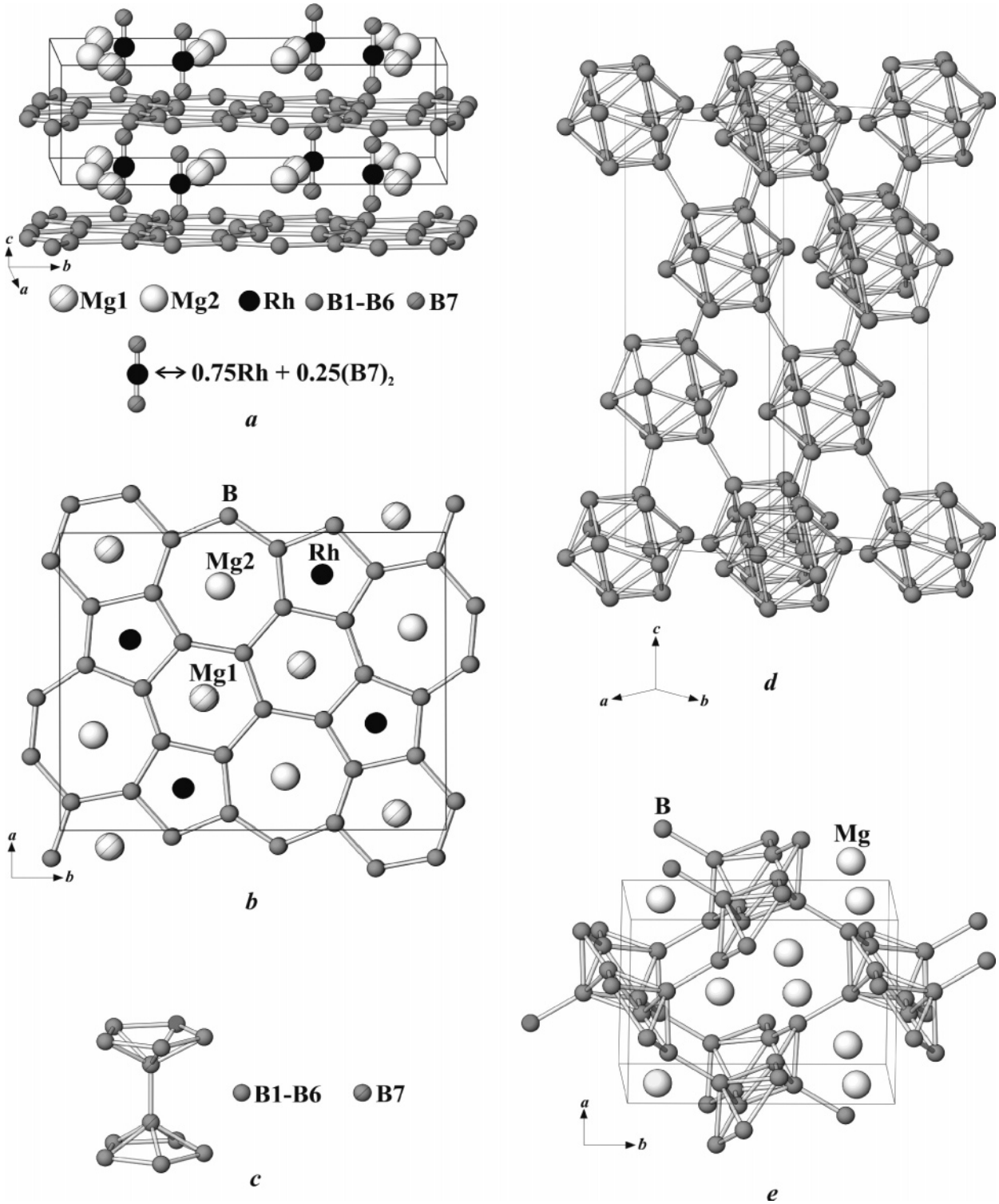

Figure 4. Crystal structure of $Mg_2Rh_{0.75}B_{6.5}$: (a) alternation of the atomic layers perpendicular to [001]; (b) [001] projection of the structure with full occupancy of the Rh position; (c) interconnection of the planar nets by the additional boron atoms in the B7 position; (d) pentagonal-pyramidal units in the crystal structure of α-boron; (e) pentagonal-pyramidal units in the crystal structure of MgB_4.

the initial composition: from $a = 8.7771(7)$ Å, $b = 11.063(1)$ Å, and $c = 3.5559(3)$ Å for $x = 0$ to $a = 8.728(1)$ Å, $b = 11.034(3)$ Å, and $c = 3.618(1)$ Å for $x = 0.9$. The variation of the lattice parameters confirms the existence of the homogeneity range for the $Mg_2Rh_{1-x}B_{6+2x}$ solid solution due to the replacement of the Rh atoms by the boron pairs, corresponding to the reduction of the cell size in the (001) plane and the expansion of the unit cell along the *c* axis. Despite several attempts, the fully equilibrated samples of the solid solution were not obtained. Therefore, the exact region of *x* in $Mg_2Rh_{1-x}B_{6+2x}$ was not established. The samples with $x = 0$ and $x = 0.9$ are definitely not single phases. For $x = 1$ the binary MgB_4 phase is known with its own crystal structure (Figure 4e).[39] Thus, the homogeneity range is located between $x = 0$ and $x = 0.9$, in any case between $x = 0.25$ and $x = 0.4$.

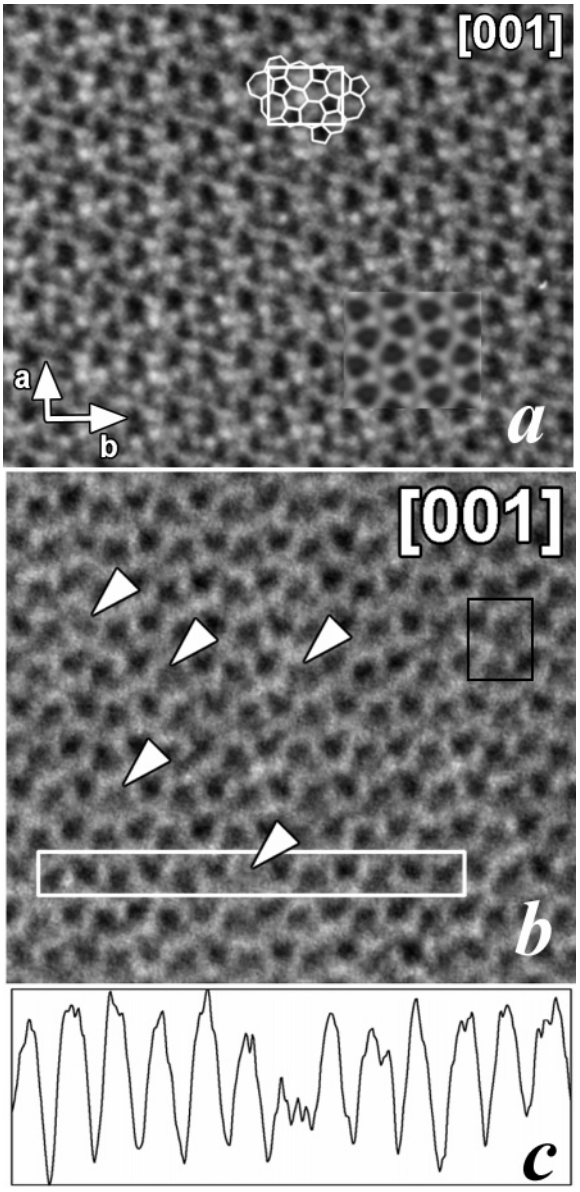

Figure 5. [001] HREM image of $Mg_2Rh_{0.6}B_{6.8}$ along [001]: (a) comparison of the experiment with the calculated image (inset), with unit cell indicated by a white rectangle and a scheme of the boron net; (b) pointlike defects (marked by arrows and with black rectangle) related to the preferential occupation of the positions by boron pairs; (c) strong contrast change along the region indicated with the white rectangle in (b).

Two models of the bonding pattern in $Mg_2Rh_{1-x}B_{6+2x}$ were investigated: Mg_2RhB_6 with the unmodified Y_2ReB_6 structure; $Mg_2Rh_{0.5}B_7$ with ordered substitution of half of the rhodium atoms by boron pairs (space group $P2_1am$). In both cases, the lattice parameters of $Mg_2Rh_{0.75}B_{6.5}$ (Table 1) were used.

The total electronic density of states (DOS) for both models is presented on Figure 6. In both cases the Fermi level lies in a pseudogap with very small value of DOS. In vicinity of E_F, DOS is mainly constructed of B(p) states and Rh(d) states. Since the DOS does not change remarkably with rhodium-by-boron pair substitution, a further investigation of the chemical bonding was undertaken using the combined topological analysis of the electron localization function and electron density.

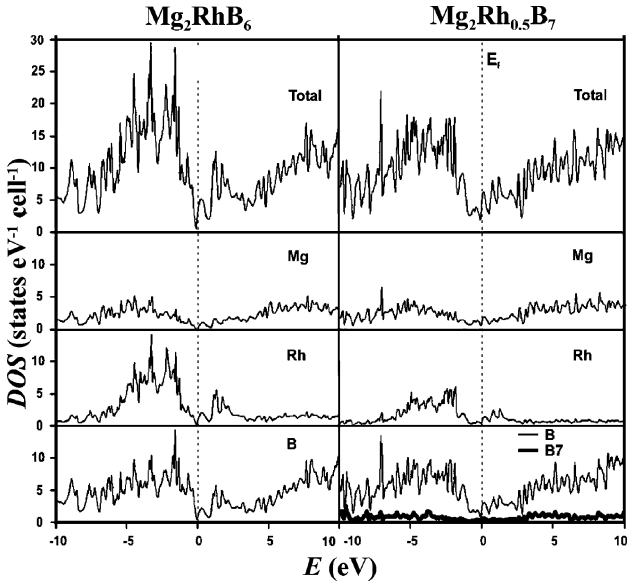

Figure 6. Electronic density of states for the model structures Mg_2RhB_6 and $Mg_2Rh_{0.5}B_7$. Partial contributions of the B7 atoms are highlighted on the right side

The electron localization function for the Mg_2RhB_6 model (space group *Pbam*) is shown in Figure 7a. Each of the B−B contacts within the planar boron nets has an attractor in the ELF representation revealing two-center bonding. All boron atoms are three-bonded. The presence of pentagonal, hexagonal, and heptagonal boron rings and hence the different bond lengths and angles inside the boron net are reflected by the variation in their electron counts in the range of 2.43−3.23 e^-. The electron counts do not correlate with the according interatomic distances, which is often for ELF representations. Nevertheless, the average value of the electron count for the whole net is 2.67 e^-/bond, which exactly matches the Zintl count, in contrast to 2.5 e^-/B−B bond found in the MgB_2 compound[48] but in agreement with the results on AlB_2.[49] The formal charge of the crystallographically different boron atoms (within the homolytic cleavage approach) varies from −0.94 to −1.15 with the average value of −1.02.

No unique attractors were found between Mg or Rh and the boron atoms, indicating the ionic interaction between the anionic boron network and the cations. It should be noted that, in contrast to this case, in other ternary magnesium rhodium borides such as $Mg_{1-x}RhB$[45] and Mg_8Rh_4B[50] covalent Rh−B interactions were observed. The charges of the Mg and Rh atoms for the Mg_2RhB_6 model were found to be +2 within the accuracy of the calculations ($Mg^{+1.96}$ and $Rh^{+1.97}$).

Thus, the formal electron balance for the Mg_2RhB_6 model can be written as $[Mg^{2+}]_2[Rh^{2+}][B^{1-}]_6$. A transfer of six electrons/formula unit from the metal atoms to the boron

(48) Schmidt, J.; Schnelle, W.; Grin, Yu.; Kniep, R. *Solid State Sci.* **2003**, *5*, 535.
(49) Burkhardt, U.; Gurin, V.; Haarmann, F.; Borrmann, H.; Schnelle, W.; Yaresko, A.; Grin, Yu. *J. Solid State Chem.* **2004**, *177*, 389.
(50) Alekseeva, A. M.; Abakumov, A. M.; Leithe-Jasper, A.; Schnelle, W.; Prots, Yu.; Chizhov, P. S.; Van Tendeloo, G.; Antipov, E. V.; Grin, Yu. *J. Solid State Chem.* **2006**, *179*, 2751.

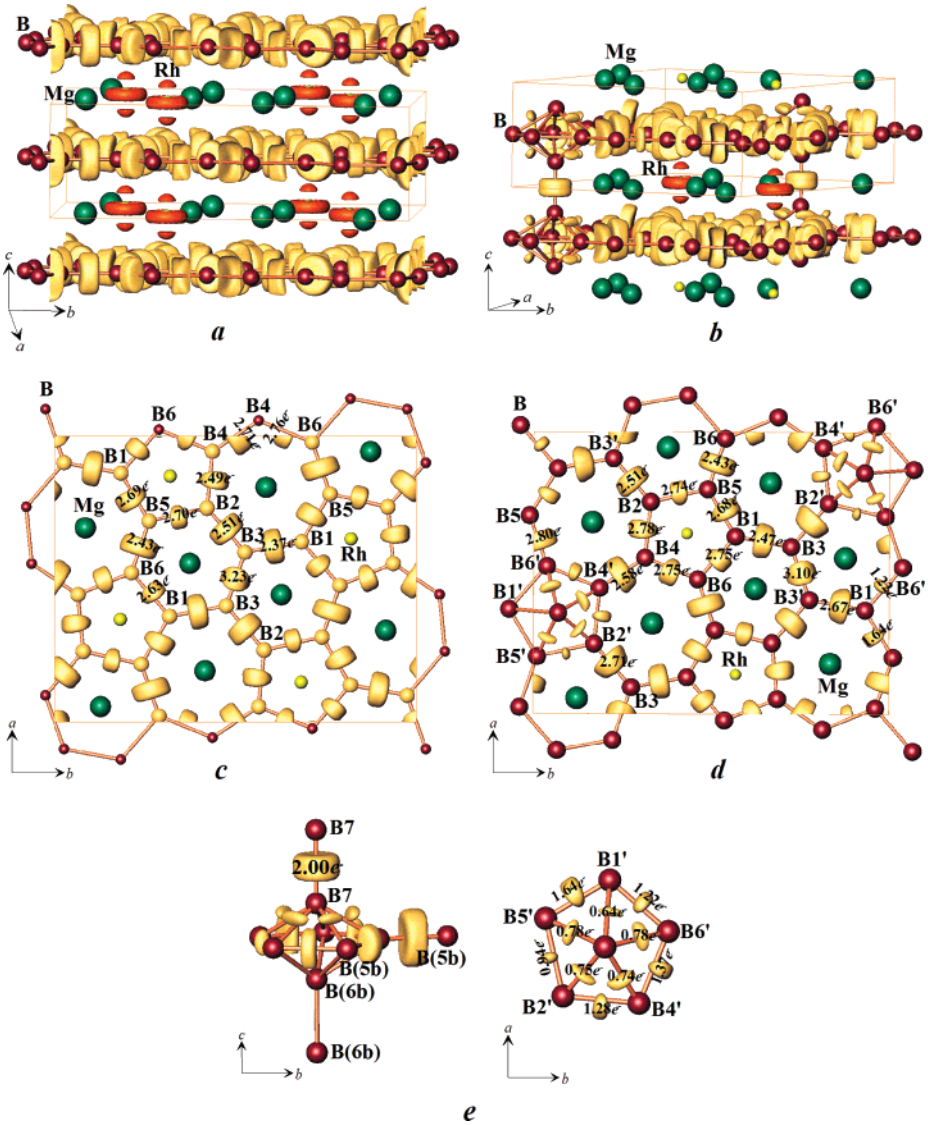

Figure 7. Electron localization function for the (a) Mg_2RhB_6 and (b) $Mg_2Rh_{0.5}B_7$ models (isosurfaces with $\eta = 0.75$ in yellow and $\eta = 0.65$ in brown-orange shown). (c) ELF distribution and electron counts within the planar boron net in Mg_2RhB_6. (d) ELF distribution and electron counts within the planar boron network in $Mg_2Rh_{0.5}B_7$. (e) B-B bonds in the pentagonal pyramidal unit and between boron atoms of the B7−B7 pair.

net is necessary. The formation of vacancies in the rhodium position leads to an electron deficiency in the polyanion that should be compensated, e.g., by implementing of B−B pairs.

To elucidate the changes in the chemical bonding with rhodium-by-boron pair substitution, the ELF distribution in the $Mg_2Rh_{0.5}B_7$ model (space group $P2_1am$) was calculated and analyzed (Figure 7b; the boron atoms connected to the pair $(B7)_2$ are marked as $B_{i'}$). It demonstrates similar main features as in the Mg_2RhB_6 model. Covalent boron-boron interaction exists in the boron network; magnesium and rhodium atoms do not form covalent bonds with boron. The boron polyanion in the $Mg_2Rh_{0.5}B_7$ model is formed by the three-bonded boron atoms (B(3b)) from the planar nets, the five-bonded boron atoms (B(5b)) forming the vertices of the pentagonal rings, and the six-bonded boron atoms (B(6b)) constituting the boron pairs. The electron count for the bonds between the three-bonded boron atoms lies in the range of 2.43−3.10 e^-, with the average value of 2.69 e^-, quite close to that in the Mg_2RhB_6 model. The introduction of boron pairs leads to additional bonds with much smaller electron counts (Figure 7d,e). The electron counts for the B(5b)−B(5b) bonds are in the range 0.94−1.64 e^- with the average value of 1.29 e^-/bond. The B(6b)−B(5b) boron-boron interactions are characterized by smaller electron counts (0.60−0.78 e^-/bond with the average value of 0.73 e^-), whereas the B(6b)−B(6b) bond inside the pair is a simple two-electron bond. The average formal charges of boron atoms of different types calculated within the homolytic cleavage approach are −1.10 for three-bonded boron atoms, −0.44 for five-bonded boron atoms, and +0.08 for six-bonded boron atoms. Charges of Mg and Rh atoms remain the same, as in the Mg_2RhB_6 model ($Mg^{1.98+}$ and $Rh^{1.97+}$). The distortion of the Rh outer core shell also does not change with rhodium-by-boron pair substitution, confirming the same character of the Rh−B interactions in both structures.

These data allow the deducing of the formal electron balance for $Mg_2Rh_{0.5}B_7$:

$$[Mg^{2+}]_2[Rh^{2+}]_{0.5}[B(3b)^{1.10-}]_{3.5}[B(5b)^{0.44-}]_{2.5}[B(6b)^{0.08+}]_1 =$$

$$[Mg^{2+}]_2[Rh^{2+}]_{0.5}[B_7]^{4.87\approx5.0-}$$

The appearance of the boron pairs instead of the Rh atoms and, hence, the formation of the 3D boron framework result in a formal charge rearrangement within the boron framework, while the total electron transfer from the cations to the boron polyanion does not change. Consequently, the boron pairs in the $Mg_2Rh_{0.5}B_7$ structure stabilize the Y_2ReB_6 structure motif in case of Rh deficiency. In other words, the introduction of the boron pair compensates the electron deficiency caused by the appearance of the rhodium vacancies through the formation of covalent B−B bonds with low electron count. From this point of view, a homogeneity range $Mg_2Rh_{1-x}B_{6+2x}$ may exist, which is supported by experimental results.

Replacement of the metal atoms by boron pairs may be favored by the small r_{RE}/r_M ratio (RE = Sc, Y). Concerning the lower boundary of this size ratio, the smallest known value was found in the Sc_2AlB_6 compound ($r_{Sc}/r_{Al} \sim 1.147$). The structure of Sc_2AlB_6 was refined from single-crystal X-ray diffraction data with a slightly substoichiometric occupation (90(1)%) of the Al position along with anisotropic displacement.[17,18] Small residual electron density peaks were also observed above and below the Al position. These facts may suggest that near or below the lower boundary of the metal size ratio the Y_2ReB_6 structure can be stabilized with boron-pair substitution.

The measurements of physical properties were performed on the good quality bulk sample mentioned above with the initial $Mg_2Rh_{0.5}B_7$ composition. Corresponding to the results of single-crystal structure solution and the results of the EDXS measurements performed for this sample, the composition can be written as $Mg_2Rh_{0.6}B_{6.8}$. The corrected magnetic susceptibility $M(T)/H$ is diamagnetic and shows traces of paramagnetic impurities at low temperatures. At 300 K a value of $-85(50) \times 10^{-6}$ emu·mol^{-1} is found. Thus, no Pauli paramagnetic contribution is detected in $Mg_2Rh_{0.6}B_{6.8}$. No superconductivity or other phase transitions were observed in the temperature range investigated.

The electrical resistivity $\rho(T)$ of the compound (ca. 3.0 mΩ cm at room temperature) varies only little with temperature ($\rho(300\ K) - \rho_0 \approx 0.2$ mΩ cm). Interestingly, a broad rounded minimum of $\rho(T)$ is visible at ca. 45 K which is followed by a gradual transition toward a linear increase above 120 K. The magnitude and the temperature dependence of $\rho(T)$ are reminiscent of a continuous metal−insulator transition, which is additionally smeared out by the rhodium/boron pairs disorder. In tendency, this is in agreement with the results of the band structure calculations, revealing a narrow pseudo gap for Mg_2RhB_6 composition and showing an increase of the DOS at Fermi level for $Mg_2Rh_{0.5}B_7$.

Conclusions

The crystal structure of $Mg_2Rh_{1-x}B_{6+2x}$ represents a first example of a modified Y_2ReB_6 type structure. The random replacement of the rhodium atoms by boron pairs allows the adaptation of the crystal structure to the electron deficiency caused by the vacancies in the rhodium position and to keep the main structural motif. According to the chemical bonding analysis with electron localization function, the electron deficiency is compensated by the formation of the new B−B covalent bonds between the planar nets with lower electron counts. In agreement with the band structure calculations, the compound is diamagnetic with a relatively high electrical resistivity.

Acknowledgment. We thank Dr. Gudrun Auffermann and Mrs. Ulrike Schmidt for the chemical analysis, Mrs. Susann Müller for the DTA/DSC, and Mr. R. Koban for physical measurements. Dr. Ulrich Burkhardt is acknowledged for the metallographic analysis. Mrs. Katja Schulze is thanked for the EDXS measurements. This work was partially supported by the RFBR (Grant 06-03-33066-a).

Supporting Information Available: Structural, electrical resistivity, and magnetic susceptibility data. This material is available free of charge via the Internet at http://pubs.acs.org.

IC7004453